Journal of Ceramic Processing Research. Vol. 6, No. 4, pp. 326~331 (2005)

J O U R N A L O F
Ceramic Processing Research

A model of fracture toughness in fibrous Si_3N_4 monolithic ceramics

Hai Guo, Dae-Hyun Yoon[a] and Dong-Woo Shin[a,]*

Department of Materials Science and Engineering, Division of Ceramics, Tsinghua University, Beijing, 100084 China
[a]Ceramic Matrix Composites (CMCs) Lab. Division of Materials Science and Engineering, Engineering Research Institute, Gyeongsang National University, Jinju, Gyeongnam 660-701, Korea

A fracture toughness model describing the fracture behavior of fibrous monolithic ceramics, based on the analysis of the energy of interfacial cracks is presented. The results reveal that the only factor that contributes to the fracture toughness in ceramics was the actual energy absorbed by crack propagation and not the total work of fracture. The load-displacement curve and the crack propagation path were predicted using a derived model which was the mirror image with that of the experimental data. The influence of unit cell dimension, strength, and interfacial bonding strength on properties of the ceramics were predicted using a fracture toughness model which matched with the experimental results. The deviation in results was less than 10% which indicates the validity of the proposed model.

Key words: Fracture toughness model, Fibrous monolithic ceramics, Actual energy absorbed by crack propagation.

Introduction

Since Coblenz [1] invented a way to fabricate ceramic fibers, Baskaran [2-5] and co-workers have demonstrated that a fibrous monolithic ceramic is a novel method to improve the fracture toughness of ceramics. The fibers are conveniently made by spinning (or extruding) using a plastic mixture of the ceramic powder and organic binder, followed by sintering. This method lowers the cost of making fibers, and simultaneously, it conveniently controls the diameter and structure of fibers.

A prediction of the mechanical properties using a fracture toughness model helps in making high performance ceramic composites so that researchers can avoid all the lengthy experimental work and save time as well as money. Earlier, fiber reinforced ceramics have been researched in detail, and some theoretical models were proposed, based on the concept that the fibers acts as a reinforced phase with the strength of the fiber being higher than the matrix. However, in a fibrous monolithic ceramic, the fiber is not the reinforcement but consists of a matrix phase and a second phase which is an interface with <5% of the volume.

Considering the matrix and interface phase of the fiber, a model is proposed to analyze the fracture behavior of fibrous monolithic ceramics in the present investigation. Other research on modeling is also based on the analysis of the energy of interfacial cracking in laminated ceramics [6-7], which have similar fracture behavior to that of fibrous monolithic ceramics.

*Corresponding author:
Tel : +82-55-751-5332
Fax: +82-55-755-6755
E-mail: dwshin@gsnu.ac.kr

Experimental Procedures

Green fibers were used to make the fibrous Si_3N_4 monolithic ceramics. These fibers act as basic structural units separated by a meagre interface. The green fibers used in the present investigation were extruded using a plastic mixture of 12 wt% poly (vinyl) alcohol (PVA) as the organic binder, 3 wt% glycerol as the plasticising agent, and a ball-milled mixture of 55 wt% α-Si_3N_4 (Founder Corporation, Beijing, China), 7 wt% Y_2O_3 (purity > 99.9%, Hokke Chemicals, Tokyo, Japan), 3 wt% Al_2O_3 (purity > 99.9%), and 20 wt% SiC whickers (TWS-400, Hokke Chemicals, Tokyo, Japan) or 3 wt% β-Si_3N_4 seeds (in this case, 72 wt% of α-Si_3N_4 was used). The green fibers extruded with different fiber diameters were subsequently coated with a BN-Al_2O_3 slurry. These green fibers were cut and stacked in a particular order in a graphite die. The heat treatments at 260 °C for 2 h and at 400 °C for 4 h were given to remove the organic binder. Subsequently, the green body was hot pressed at 1800 °C for 1 h under a nitrogen atmosphere to give fibrous monolithic Si_3N_4.

Modeling of the Fibrous Monolithic Structure

Structure of Fibrous Monolithic Ceramic

The microstructure of the synthesized Si_3N_4/BN-Al_2O_3 fibrous monolithic ceramic is shown in Fig. 1. (SEM, CSM-950, OPTON, Germany). A plane parallel to the fiber direction is shown in Fig. 1(a), and Fig. 1(b) shows the "end view" of uniaxially aligned fibers.

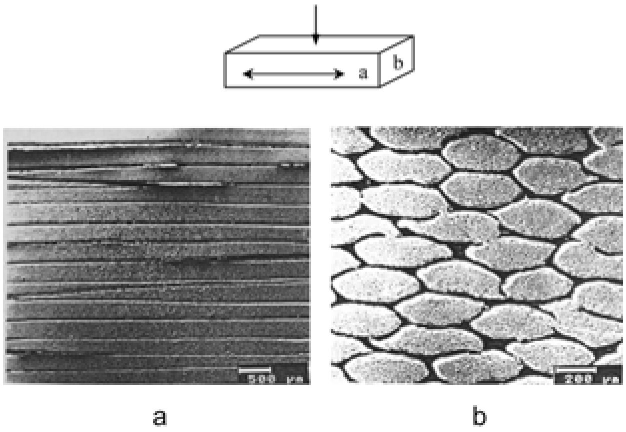

Fig. 1. SEM micrographs of macro-structure of Si_3N_4 fibrous monolithic ceramic.

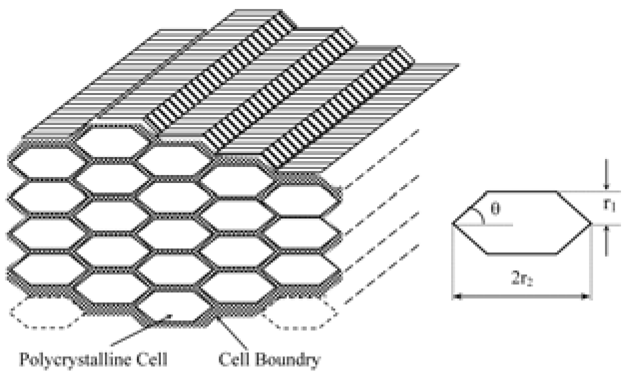

Fig. 2. Schematic illustration of fibrous monolithic structure.

The cross section of the fibers is hexagonal. The fiber boundary phase, BN, acts as a weak interface, creating a clear separation between the fiber and interface.

By analyzing the SEM photographs, we describe the structure of fibrous monolithic ceramics, as follows:

(1) The fibrous monolithic ceramics is built-up mainly of fibrous domains, which have hexagonal cross sections of identical size.

(2) The application of the weak interface separates these fibrous domains. The thickness and strength of the interface is negligible in comparison to the fibrous domains.

On the bisis of this description, a schematic of the fibrous monolithic structure is shown in Fig. 2.

Analysis of Crack formation

Two kinds of cracks exist during delamination of the structure under the flexural test. One is the breakthrough crack, which occurs in fibrous domains. When the driving force adds up to a value greater than the resistance force, breakthrough cracks are generated and propagate instantly for a length of one domain thickness, and damage one or more fibrous domains. According to the Griffith theory, the driving force is expressed as :

$$G_b = \frac{dW_b}{2bc} = \frac{\pi\sigma^2 c}{E} \qquad (1)$$

where W_b is the interfacial strain energy of the specimen, b is the specimen width, c is the length of the crack which equals the thickness of one fibrous domain, E is Young's modulus, and σ is the stress loading on the domains. Another way to evaluate the resistance force from Eq. (1) is by changing σ to σ_m, the bending strength of the fibrous domain.

Another kind of crack is an interfacial crack, which occurs at the interface. The driving force of this crack is determined by the interfacial strain energy release rate, G_i, :

$$G_i = \frac{P^2}{2b} \cdot \frac{dC}{da} \qquad (2)$$

where P is the load, C is the specimen compliance and α is the length of the interfacial crack. The resistance force is determined by the interfacial strain energy release rate, G_{ic}, which is a constant.

Analysis of the Fracture Process

The fracture process consists of two independent processes: i) brittle collapsing of a batch of fibrous domains and ii) generation and propagation of interfacial cracks. With brittle collapsing of a batch of fibrous domains, the basic structural unit consists of fibrous domains which can be divided into two types, A and B. As one breakthrough crack propagated, a batch of one type of domains get damaged (This process is called an elementary fracture.), and the breakthrough crack propagated for a length of one domain thickness. For the second elementary fracture, another type of domain gets damaged alternately. Figure 3 is a schematic illustration of the fracture process of a fibrous monolithic ceramic.

In the generation and propagation of interfacial cracks, the application of the force which causes the breakthrough cracks is higher and simultaneously induces the generation of interfacial cracks at the interface. The driving force is an order of magnitude higher than the

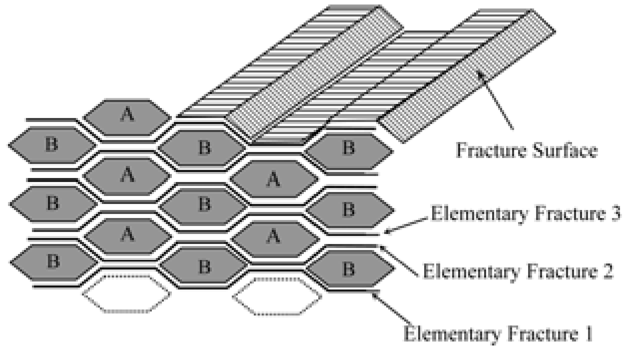

Fig. 3. Schematic illustration of the fracture process of a fibrous monolithic ceramic.

resistance force ($G_i >> G_{ic}$). Interfacial cracks propagate rapidly even at constant roller displacement. Generation and propagation of interfacial cracks absorb elastic strain energy, consequently, a descending curve of driving force appears up to the point of equilibrium of G_i and G_{ic}.

Application of further force leads to a steady propagation of the interfacial cracks. However, a driving force keeps a dynamic equilibrium with the resistance force until the force becomes high enough to cause the next elementary fracture of a fibrous domain. This process takes place alternatively until the ceramic gets completely broken through.

Analysis of Structure Under the Three-point Bend Test

A schematic of the specimen under three-point bend test is shown in Fig. 4. The breakthrough cracks occur at the center of the beam and the interfacial cracks propagate symmetrically from the center. For the convenience of calculation, the zero of the coordinate is set at the bottom of the beam so that all the deformation becomes positive. The beam is divided into two T-1 regions according to the length of each interfacial crack in different interfacial regions. T is equal to half the number of interfacial cracks, so that the mechanical calculation may be conducted individually.

The load applied on the specimen is :

$$P = U/C \tag{3}$$

where U is the roller displacement and C is the specimen compliance.

The inertia moment of the nth region (shown in Fig. 4) is given by :

$$I_n = \frac{b}{12}\cdot f(H, r_1, r_2, \theta) \tag{4a}$$

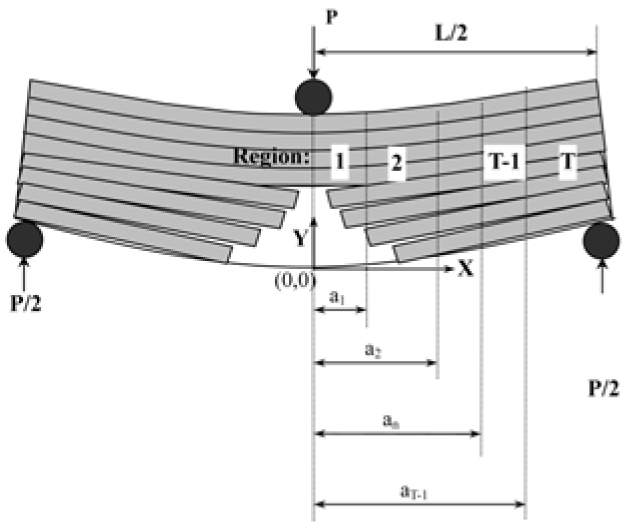

Fig. 4. Schematic illustration of specimen under three-points bending test, in which a_n is the length of nth interfacial crack.

where H is the height of the residual beam, γ_1 is half of the thickness of one fibrous cell, γ_2 is half of the width of one fibrous cell, and θ as demonstrated in Fig. 2. Equation (4a) is a simple mechanical calculation as :

$$f(H, r_1, r_2, \theta) = \frac{1}{2r_2^2}[-H\tan^{-2}\theta r_1^4 - 5Hr_2\tan^{-1}\theta r_1^3 + (6Hr_2^2 - H^3\tan^{-2}\theta)r_1^2 + (\tan^{-1}\theta - 2)H^3 r_2 r_1 + 2H^3 r_2^2] \tag{4b}$$

Using the inertial moment of each region, we can derive a theoretical expression for the specimen compliance as:

$$C = -\frac{1}{2EI_{T+1}}\left(\frac{L^3}{24} + \frac{L}{2}A_{T+1} + B_{T+1}\right) \tag{5}$$

where L is the loading span, A_{T+1} and B_{T+1} are constants particular to region T and can be calculated with the recurrence formulae :

$$A_T = \left(\frac{I_T}{I_{T-1}} - 1\right)\left(La_T - \frac{a_{T-1}^2}{2}\right) + \frac{I_T}{I_{T-1}}A_{T-1}$$

$$B_T = \left(\frac{I_T}{I_{T-1}} - 1\right)\left(\frac{a_{T-1}^3}{3} - \frac{a_{T-1}^2}{2}\right) + \frac{I_T}{I_{T-1}}B_{T-1} \tag{6}$$

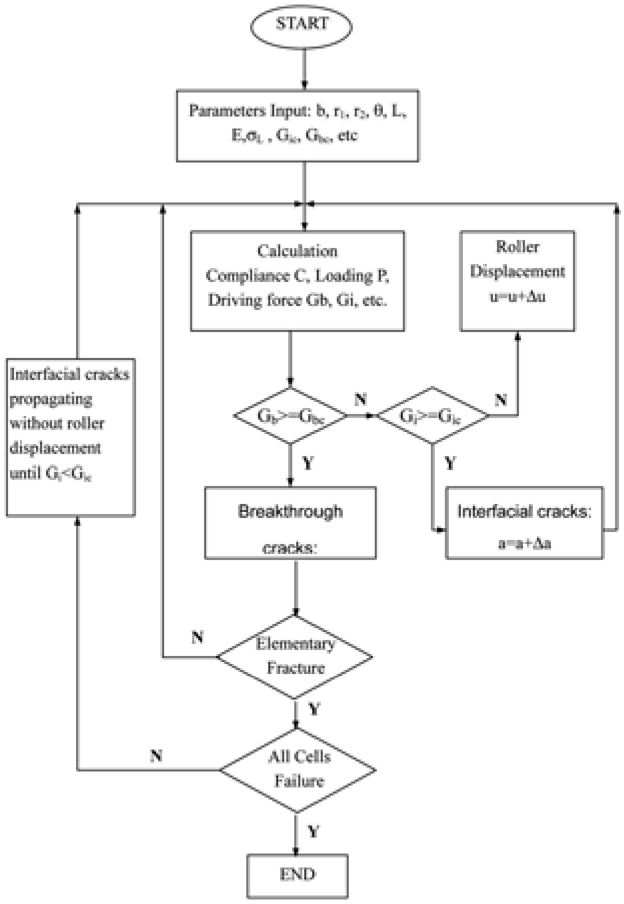

Fig. 5. Flow chart of modeling calculation program.

The loading, *P*, and the driving force of the interfacial crack is derived by differentiating the upper expression for the *T*th interfacial crack.

The proposed flow chart is shown in Fig. 5 based on the above analysis to illustrate the modeling simulation for the fracture procedure.

Comparison of Model Prediction with Experimental Data

Simulation of the Fracture Process

The predicted model load-displacement curve is presented in Fig. 6(a). This indicates that the load experienced by the test specimen decreases sharply on every elementary fracture and subsequently regains thereafter with the completion and propagation of interfacial cracks and further rises until the next elementary fracture occurs. Figure 6(b) shows the actual load-displacement curve of the test specimen which is similar to the predicted model curve. This shows that the prediction mirrors the actual fracture process.

Crack Propagating Path

Figure 7(a) shows the typical fracture behavior of the Si_3N_4/BN-Al_2O_3 fibrous monolithic ceramic. The crack is deflected at nearly every fibrous domain interface. In a real fibrous monolithic ceramic, the flexural strength is not constant everywhere along the axial line of a fiber, as assumed in our model. The breakthrough crack does not occur absolutely at the center of the beam. A Weibull distribution is employed to represent the flexural strength along the axial line of the fibrous domain. Figure 7(b) shows the predicted crack-propagating path in which the interfacial cracks propagate by oscillating from the center.

Analysis of Energy and Fracture Toughness

The total work of the loading system, calculated from the area under the load-displacement curve (Fig. 8), includes the energy absorbed by the propagating crack, the strain energy, the oscillatory energy, and the sonic energy. The total work done per unit volume is defined by :

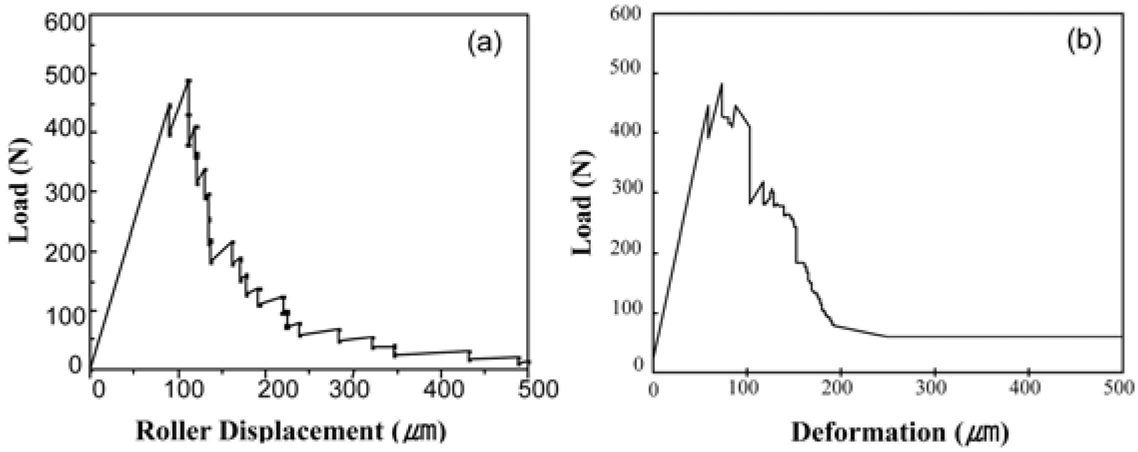

Fig. 6. Load-Displacement curve for fibrous monolithic ceramics in three-point bending test (a) Predicted by modeling calculation (b) Experimental data.

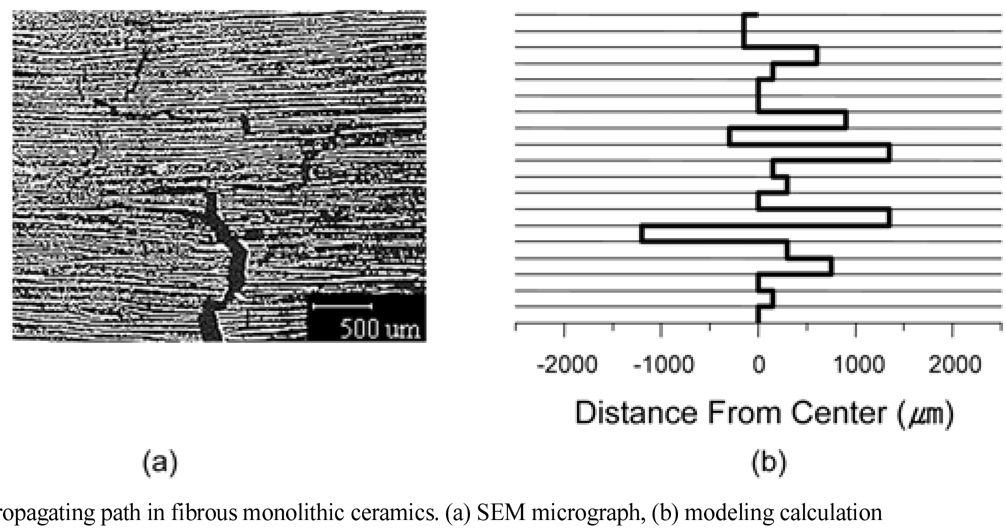

Fig. 7. Crack propagating path in fibrous monolithic ceramics. (a) SEM micrograph, (b) modeling calculation

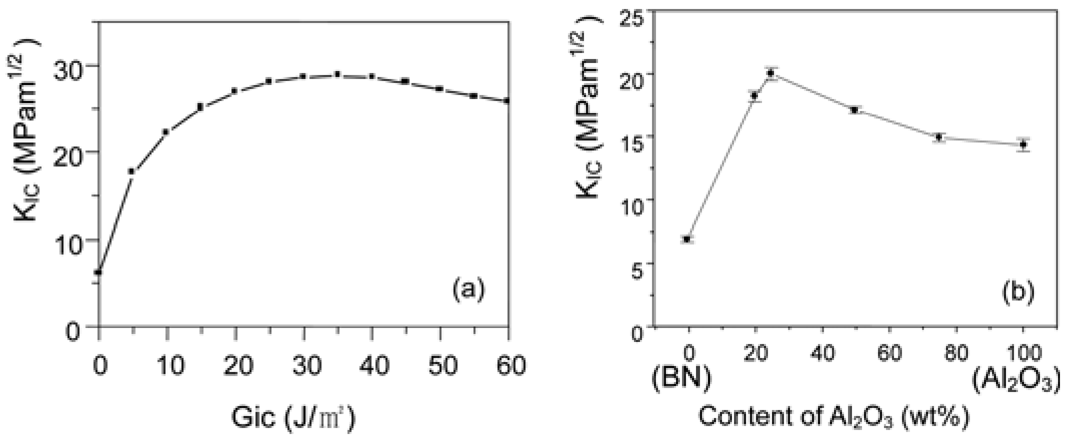

Fig. 8. Influence of strain energy of interface (G_{ic}) on toughness (a) Predicated by modeling calculation (b) Experimental data by the control of the content of Al_2O_3 in the cell boundary.

$$W = \frac{\int_0^{u_{max}} Pdu}{2Nbr + 2b\sum_{i=1}^{T} a_i} \tag{7}$$

where W is the work-of-fracture, u is the roller displacement, and N is the half number of fibrous domains.

The fracture toughness in solid mechanics is :

$$K_I = \sqrt{\frac{EW}{1-\nu^2}} \tag{8}$$

where υ is the Poisson ratio of ceramic.

Equation (7) gives fracture the toughness of a fibrous monolithic ceramics as 50 MPa·m$^{1/2}$, which is much higher than the experimental value. The reason for this difference is that the work-of-fracture consists of some energy which has no relationship with crack propagation and should not be included to calculate the fracture toughness.

Another important energy component should be noted in this context. The energy absorbed only for crack propagation, which we name it as the actual energy absorbed — W_{act}, can be defined by:

$$W_{act} = \frac{\sum_{n=1}^{T} a_n G_{ic} + NrG_{bc}}{2Nr + 2\sum_{i=1}^{T} a_i} \tag{9}$$

and the fracture toughness can be calculated:

$$K_I = \sqrt{\frac{EW_{act}}{1-\nu^2}} \tag{10}$$

The value of the fracture toughness calculated by this equation is about 20 MPa·m$^{1/2}$, which is almost equal to the value obtained experimentally.

Fracture Toughness

A comparison of the predicted model and the experimental results was made with respect to interfacial toughness and the strength and dimension of fibrous domains.

– Interfacial toughness

The influence of the strain energy of the interface, G_{ic}, on the interfacial toughness is shown in Fig. 8(a). The model predicts that G_{ic} increases exponentially to a peak and thereafter decreases nominally. This pattern reveals the interfacial toughness contributions to the fracture toughness of ceramics with weak interfaces. Since BN gives weak interfaces and Al_2O_3 gives strong interfaces, coating with different amounts of BN-Al_2O_3 were used in the present investigation to alter the magnitude of the interfacial strength. The values obtained are shown in Fig. 8(b). The curve superimposes with the curve predicted using the model, and shows 25 wt% BN + 75 wt% Al_2O_3 as an optimum interface content.

– Strength and dimension of fibrous domain

The main contribution to the fracture toughness

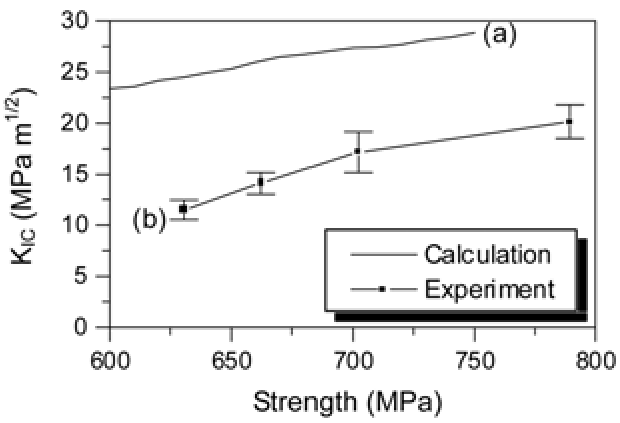

Fig. 9. Influence of the cell strength on fracture toughness. (a) modeling calculation, (b) experimental data

Table 1. Comparison of fracture toughness of Si_3N_4 fibrous monolithic ceramics both by experiment and by model predict

Diameter of Green Fiber (mm)	1.0	0.7	0.5	0.3
Bending Strength (MPa)	720.8	678.1	639.7	607.3
Fracture Toughness by Model predict (MPa $m^{1/2}$)	22.5	24.7	25.0	25.8
Fracture Toughness by Experiment (MPa $m^{1/2}$)	20.01	22.56	22.96	23.95

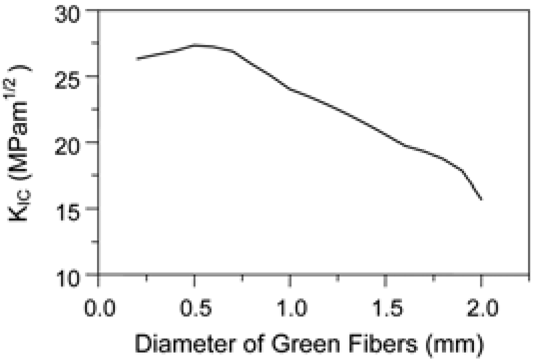

Fig. 10. Influence of average dimension of the cells on fracture toughness by the modeling calculation.

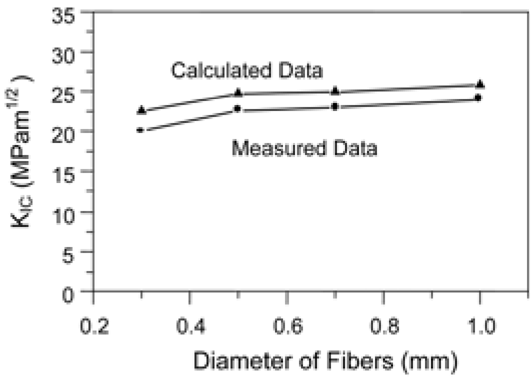

Fig. 11. Comparison of experimental results and model prediction, with the consideration of both dimension and strength of fibrous cell.

comes from the strength of the fibrous domain. Figure 9, the influence of the strength of fibrous domain on fracture toughness, reveals that the trend is the same in the predicted model and the experimental data. The difference in value may be because of the presence of the interfacial content. Both curves, the model and the experimental, reflect an improvement in fracture toughness with an increase in cell strength.

Figure 10 shows the predicted model of the influence of the average dimension of cells on fracture toughness. Since the measurement of the cell's average dimension is difficult, the green fiber diameter is used to represent the cell dimension.

Each and every parameter individually all affect concurrently the fracture toughness. Table 1 and Figure 11 show the results predicted on the basis of the proposed model and those obtained through experimental data. The deviation in results is quite small which implies the validity of the proposed model.

Conclusions

This investigation demonstrates that :

i) The proposed model describing the fracture toughness is valid in the fibrous Si_3N_4 monolithic ceramic case.

ii) W_{act} by crack propagation defines the fracture toughness in ceramics, instead of the work of fracture.

iii) The unit cell dimension, strength, and interfacial bonding strength play deciding roles in the properties of the ceramics.

Acknowledgement

This work was supported by the Japan-Korea Core University Program entitled "New Processing and Nanostructure/Property Relationship of Multi-functional Ceramic Materials

References

1. W.S. Coblenz, U.S. Patent 4772524, 20[9] (1988).
2. S. Baskaran, S.D. Nunn, and J.W. Halloran, J. Am. Ceram. Soc. 76[9] 2217-24 (1993).
3. S. Baskaran, and J.W. Halloran, J. Am. Ceram. Soc. 76[9] 2225-32 (1993).
4. S. Baskaran, and J.W. Halloran, J. Am. Ceram. Soc. 77[5] 1249-55 (1994).
5. S. Baskaran, and J.W. Halloran, J. Am. Ceram. Soc. 77[5] 1256-62 (1994).
6. A.J. Phillipps, W.J. Clegg, and T.W. Clyne, Acta Metall. Mater. 41[3] 805-817 (1993).
7. A.J. Phillipps, W.J. Clegg, and T.W. Clyne, Acta Metall. Mater. 41[3] 819-827 (1993).